J. Fluid Mech. (1971), *vol.* 46, *part* 3, *pp.* 465–475
Printed in Great Britain

Potential flow of segmental jet deflectors

By H. Y. CHANG AND J. F. CONLY
San Diego State College, San Diego, California

(Received 7 July 1970)

A solution is developed for the deflexion of an inviscid, incompressible, two-dimensional jet by a series of segments of arbitrary number, lengths, and angles. The Schwarz–Christoffel transformation and free-streamline theory are used. Results are calculated for a number of configurations, using an IBM 360 computer. Excellent comparison is found with several previous calculations for special cases.

1. Introduction

The deflexion of jets by segmental deflectors is a matter of importance in a number of applications. In hydraulics one encounters water jets deflected by gates, flip buckets on spillways (Tinney *et al.* 1961), or other obstacles. In aerodynamics air streams are deflected by control surfaces and spoilers. Recently there has been considerable interest in jet deflexion by thrust reversers on aircraft engines (Chang 1968). Segmental deflectors may also be used for pelton wheels.

The problem of an ideal two-dimensional jet, deflected by a series of straight segments, lends itself to solution by the Schwarz–Christoffel transformation. The solution relates the deflexion angle of a jet to the lengths of the deflector segments and the turning angles between them, as shown in figure 1. Some special cases, for one and two segments, have been solved by previous investigators. The one-segment deflector was solved by Siao & Hubbard (1953). The two-segment deflector was first solved by Sarpkaya (1953), with the turning angles between segments limited to 90 degrees; and later by Tinney *et al.*, for any two equal turning angles between segments. The present paper gives a solution for any number of segments at arbitrary turning angles.

2. Conformal transformation of the flow region

The flow boundary consists of two parts, the free streamline and the segments. A pair of transformations are made, as shown in figure 1. The first transforms the flow region in the z plane (the physical plane) to the corresponding region in the Ω plane. The second transforms from the Ω plane onto the upper half of the t plane by the Schwarz–Christoffel transformation. Since the flow is from point E to point F in the z plane, the complex potential of the flow can be obtained in the t plane by the superposition of a point source at E and a point sink at F.

If the complex potential is ω, then the complex velocity

$$\left.\begin{aligned}\zeta &= d\omega/dz \\ \text{and}\quad \zeta &= u - iv = qe^{-i\theta},\end{aligned}\right\} \tag{1}$$

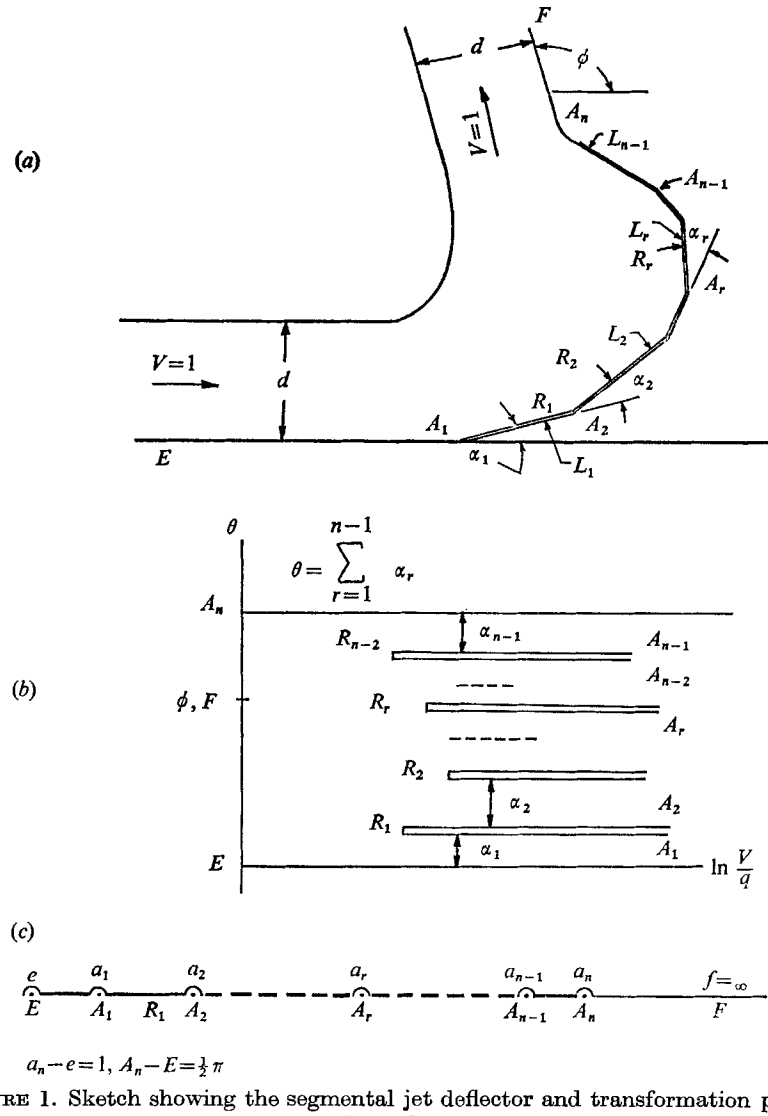

FIGURE 1. Sketch showing the segmental jet deflector and transformation planes. (*a*) z plane, (*b*) Ω plane, (*c*) t plane.

in which u and v are the velocity components in the horizontal and vertical directions respectively, and q and θ are the magnitude and inclination of the velocity vector.

The equation

$$\Omega = \ln(V/\zeta) = \ln(V/q) + i\theta \tag{2}$$

maps the flow region of the z plane onto the indicated region of the Ω plane in figure 1. In the Ω plane, points of unit velocity ($q = V = 1$) E, A_n, F are on the vertical axis, stagnation points ($q = 0$) $A_1, A_2, \ldots, A_r, \ldots$, and A_{n-1} are at infinity

in the direction of the horizontal axis. Points $R_1, R_2, \ldots, R_r, \ldots$, and R_{n-1} represent the points of maximum velocities along all the segments in the z plane.

The Schwarz–Christoffel transformation is employed to map the boundary in the Ω plane onto the real axis of the t plane, and the closed region in the Ω plane onto the upper half of the t plane. The Schwarz–Christoffel transformation for the flow under consideration is

$$\frac{d\Omega}{dt} = \frac{\text{const.}\,(t-p_1)(t-p_2)\ldots(t-p_r)\ldots(t-p_{n-1})}{(t-a_1)(t-a_2)\ldots(t-a_r)\ldots(t-a_{n-1})[(t-e)(t-a_n)]^{\frac{1}{2}}}, \tag{3}$$

in which $p_1, p_2, \ldots, p_r, \ldots$, and p_{n-1} are the t values corresponding to $R_1, R_2 \ldots, R_r, \ldots$, and R_{n-1}; the a's are the t values corresponding to the A's. Separating the above equation by partial fractions, one obtains

$$\frac{d\Omega}{dt} = \frac{1}{[(t-e)(t-a_n)]^{\frac{1}{2}}}\left[\frac{\text{const.}}{t-a_1}+\frac{\text{const.}}{t-a_2}+\ldots+\frac{\text{const.}}{t-a_r}+\ldots+\frac{\text{const.}}{t-a_{n-1}}\right]. \tag{4}$$

In order to integrate the above equation, a transformation of variable method is used. Considering only the first partial fraction

$$\frac{d\Omega_1}{dt} = \frac{\text{const.}}{(t-a_1)[(t-e)(t-a_n)]^{\frac{1}{2}}}$$

and letting $\chi = 1/(t-a_1)$ and integrating, one obtains

$$\Omega_1 = \text{const.}\int \frac{d\chi}{[(a_1-e)(a_1-a_n)\chi^2+(2a_1-e-a_n)\chi+1]^{\frac{1}{2}}}$$

$$= \text{const.}\ln\frac{[(t-a_n)(e-a_1)]^{\frac{1}{2}}+[(t-e)(a_n-a_1)]^{\frac{1}{2}}}{(t-a_1)^{\frac{1}{2}}}.$$

Thus (4) becomes

$$\Omega = C_1\ln\frac{[(t-a_n)(e-a_1)]^{\frac{1}{2}}+[(t-e)(a_n-a_1)]^{\frac{1}{2}}}{(t-a_1)^{\frac{1}{2}}}$$

$$+C_2\ln\frac{[(t-a_n)(e-a_2)]^{\frac{1}{2}}+[(t-e)(a_n-a_2)]^{\frac{1}{2}}}{(t-a_2)^{\frac{1}{2}}}+\ldots$$

$$+C_r\ln\frac{[(t-a_n)(e-a_r)]^{\frac{1}{2}}+[(t-e)(a_n-a_r)]^{\frac{1}{2}}}{(t-a_r)^{\frac{1}{2}}}+\ldots$$

$$+C_{n-1}\ln\frac{[(t-a_n)(e-a_{n-1})]^{\frac{1}{2}}+[(t-e)(a_n-a_{n-1})]^{\frac{1}{2}}}{(t-a_{n-1})^{\frac{1}{2}}}, \tag{5}$$

where the C's are constants. Referring to figure 1, when $a_{n-1} < t < a_n$, the right-hand side of (5) is real, hence from (2) and (5)

$$\theta = 0.$$

This is along the last segment or L_{n-1}.

Again, when $a_{n-2} < t < a_{n-1}$, C_{n-1} in (5) is imaginary while all the others are real, hence from (2) and (5)

$$C_{n-1}\ln 1/i = \theta.$$

Therefore

$$\theta = C_{n-1}(-\tfrac{1}{2}\pi). \tag{6}$$

This is along segment L_{n-2}.

Similarly, when $a_{n-3} < t < a_{n-2}$, C_{n-1} and C_{n-2} are imaginary and

$$(C_{n-1}+C_{n-2})\ln 1/i = -(C_{n-1}+C_{n-2})\tfrac{1}{2}\pi = \theta. \tag{7}$$

If $\theta = 0$ along the last segment, the values of θ along the two preceding segments are $-\alpha_{n-1}$ and $-(\alpha_{n-1}+\alpha_{n-2})$ respectively. Therefore, from (6) and (7), one has

$$C_{n-1} = 2\alpha_{n-1}/\pi$$

and

$$C_{n-2} = 2\alpha_{n-2}/\pi.$$

Hence for the rth segment

$$C_r = 2\alpha_r/\pi. \tag{8}$$

Substituting the values of the C's into (5), it becomes

$$\Omega = \sum_{r=1}^{r=n-1} \frac{2\alpha_r}{\pi} \ln \frac{[(t-a_n)(e-a_n)]^{\frac{1}{2}} + [(t-e)(a_n-a_r)]^{\frac{1}{2}}}{(t-a_r)^{\frac{1}{2}}}. \tag{9}$$

Referring to figure 1, with $a_n > a_{n-1} > \ldots > a_r > \ldots a_2 > a_1 > e$ in the t plane, if the scale of representation is chosen such that $a_n - e = 1$; then there exists a real angle U between $\frac{1}{2}\pi$ and zero such that $a_n - t = \cos^2 U$ and $t - e = \sin^2 U$. Thus we have

$$t - a_r = \sin^2 U - \sin^2 A_r = \sin(U+A_r)\sin(U-A_r),$$

$$[(t-a_n)(e-a_r)]^{\frac{1}{2}} + [(t-e)(a_n-a_r)]^{\frac{1}{2}}$$

$$= \cos U \sin A_r + \sin U \cos A_r = \sin(U+A_r).$$

Hence (9) becomes

$$\Omega = \sum_{r=1}^{r=n-1} \ln \left[\frac{\sin(U+A_r)}{\sin(U-A_r)}\right]^{\alpha r/\pi}. \tag{10}$$

Deflexion angle

The deflexion angle ϕ corresponds to the inclination of the velocity vector at F where $t = \infty$. Putting $t = \infty$ in (9), one has

$$\Omega = \sum_{r=1}^{r=n-1} \frac{2\alpha_r}{\pi} \ln[(e-a_r)^{\frac{1}{2}} + (a_n-a_r)^{\frac{1}{2}}] = \ln \frac{V}{q} + i\theta. \tag{11}$$

Since $a_r > e$, the imaginary part of (11) is

$$\sum_{r=1}^{r=n-1} \ln[i\sin A_r + \cos A_r] \exp\left(\frac{2\alpha_r}{\pi}\right) = i\theta.$$

$$\sum_{r=1}^{r=n-1} \ln[\exp(iA_r)] \exp\left(\frac{2\alpha_r}{\pi}\right) = \sum_{r=1}^{r=n-1} i\frac{2\alpha_r}{\pi} A_r = i\theta.$$

Therefore

$$\theta = \sum_{r=1}^{r=n-1} \frac{2\alpha_r}{\pi} A_r. \tag{12}$$

This is the inclination of the velocity vector at F when $\theta = 0$ along the last segment. Hence, from figure 2, the deflexion angle is obtained

$$\phi = \sum_{r=1}^{r=n-1} \alpha_r - \sum_{r=1}^{r=n-1} \frac{2\alpha_r}{\pi} A_r,$$

or

$$\phi = \sum_{r=1}^{r=n-1} \left(\alpha_r - \frac{2\alpha_r}{\pi} A_r\right). \tag{13}$$

Segmental lengths

The segmental length for the rth segment can be obtained from the integral

$$L_r = \int_{a_r}^{a_{r+1}} \left| \frac{dz}{dt} \right| dt.$$

The equivalent expression with the angle as the variable for the rth segment is

$$L_r = \int_{A_r}^{A_{r+1}} \left| \frac{dz}{dU} \right| dU; \tag{14}$$

for the last segment

$$L_{n-1} = \int_{A_{n-1}}^{\frac{1}{2}\pi} \left| \frac{dz}{dU} \right| dU. \tag{15}$$

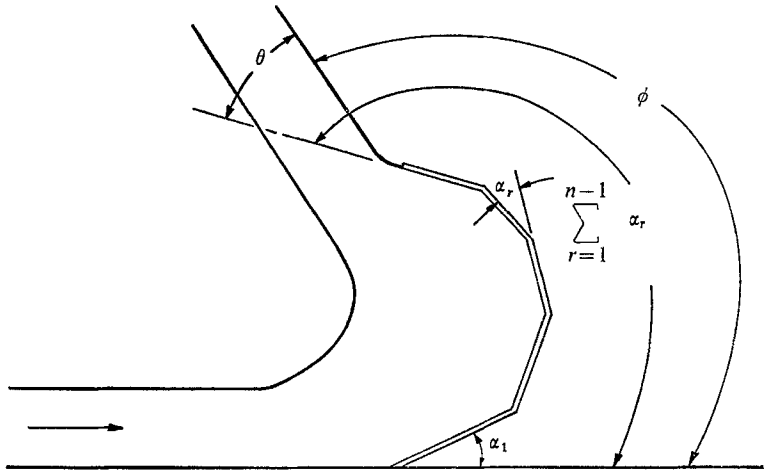

FIGURE 2. Sketch-angle relation.

The complex potential in the t plane is obtained from the superposition of a source at 'e' and a sink at 'f', or

$$\omega = (Vd/\pi)\,[\ln(t-e) - \ln(t-f)]. \tag{16}$$

Now,

$$\zeta = d\omega/dz$$

and $f = \infty$, therefore

$$dz = \frac{1}{\zeta}\frac{d\omega}{dt}\,dt$$

$$= \frac{1}{\zeta}\frac{Vd}{\pi}\left(\frac{1}{t-e} - \frac{1}{t-f}\right)dt$$

$$= \frac{1}{\zeta}\frac{Vd}{\pi}\frac{dt}{t-e} = \frac{1}{\zeta}\frac{Vd}{\pi}\frac{d\sin^2 U}{\sin^2 U}$$

$$= \frac{2}{\zeta}\frac{Vd}{\pi}\cot U\,dU. \tag{17}$$

From (2)

$$V/\zeta = e^{\Omega},$$

hence, from (10)
$$\frac{V}{\zeta} = \prod_{r=1}^{r=n-1} \left[\frac{\sin(U+A_r)}{\sin(U-A_r)}\right] \exp\left(\frac{\alpha_r}{\pi}\right). \tag{18}$$

From (17) and (18), one obtains

$$dz = \frac{2d}{\pi}\left\{\prod_{r=1}^{r=n-1} \left[\frac{\sin(U+A_r)}{\sin(U-A_r)}\right] \exp\left(\frac{\alpha_r}{\pi}\right)\right\} \cot U\, dU.$$

Substituting the above equation into (14), the segmental length is obtained

$$\frac{L_r}{d} = \frac{2}{\pi}\int_{A_r}^{A_{r+}} \left\{\prod_{r=1}^{r=n-1} \left[\left|\frac{\sin(U+A_r)}{\sin(U-A_r)}\right|\right] \exp\left(\frac{\alpha_r}{\pi}\right)\right\} \cot U\, dU. \tag{19}$$

Equation (19) is an improper trigonometric integral since it has a singularity at $U = A_r$. An approximation method (see appendix) will be used to evaluate the integral around the singularity.

Equations (13) and (19) are the resulting equations of the mathematical model. By assigning the number of segments, turning angles between segments, and values of A_r, one can obtain the deflexion angle of jets from (13) and segmental lengths from (19).

3. Results

An IBM 360 digital computer has been used to evaluate the deflexion angle (from (13)) and the segmental lengths (from (19) and the approximation method given in the appendix) for segmental deflectors with 1, 2, 3 and 5 segments. Various turning angles have also been assigned for each case. Some representative results are presented in figures 3 to 6 for one-, two- and three-segment cases. Due to the large number of variables involved for the five-segment deflector the results are not shown graphically, but some representative ones are tabulated, as shown in table 1.

Input					Results					
A_1	A_2	A_3	A_4	A_5	L_1/d	L_2/d	L_3/d	L_4/d	L_5/d	ϕ degrees
0·001	0·05	0·15	0·25	0·35	2·002	1·019	5·644	7·240	0·849	67·35
0·001	0·05	0·15	0·25	1·50	1·985	0·976	5·101	2·583	0·002	56·37
0·05	0·25	0·35	0·75	0·85	1·394	0·374	2·416	3·374	0·249	53·51
0·15	0·35	0·55	0·75	1·20	0·819	0·478	1·770	1·608	0·057	46·35
0·25	0·35	0·55	0·75	1·20	0·388	0·501	1·815	1·629	0·057	45·40
0·25	0·35	0·55	1·20	1·50	0·368	0·458	1·302	0·418	0·002	38·24

TABLE 1. Some selected results for the five-segment case with $\alpha_1 = \alpha_2 = \alpha_3 = \alpha_4 = \alpha_5 = 15°$

The results for the one-segment deflector (figure 3) have been compared with the theoretical results obtained by Siao & Hubbard. The agreement is extremely good. The theoretical results for two-segment deflectors by Sarpkaya are limited to the

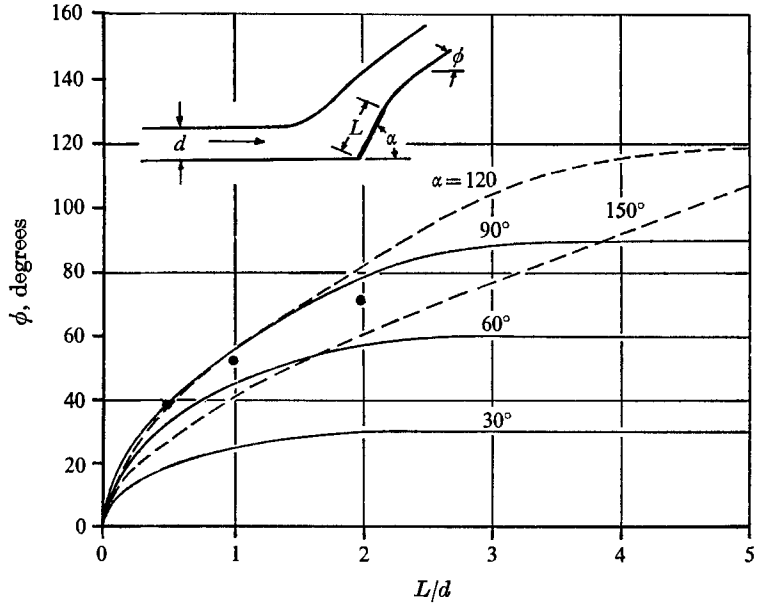

FIGURE 3. Deflexion angle as a function of segmental length and turning angle for one-segment case. ●, experimental points, $\alpha = 90°$ (Siao & Hubbard).

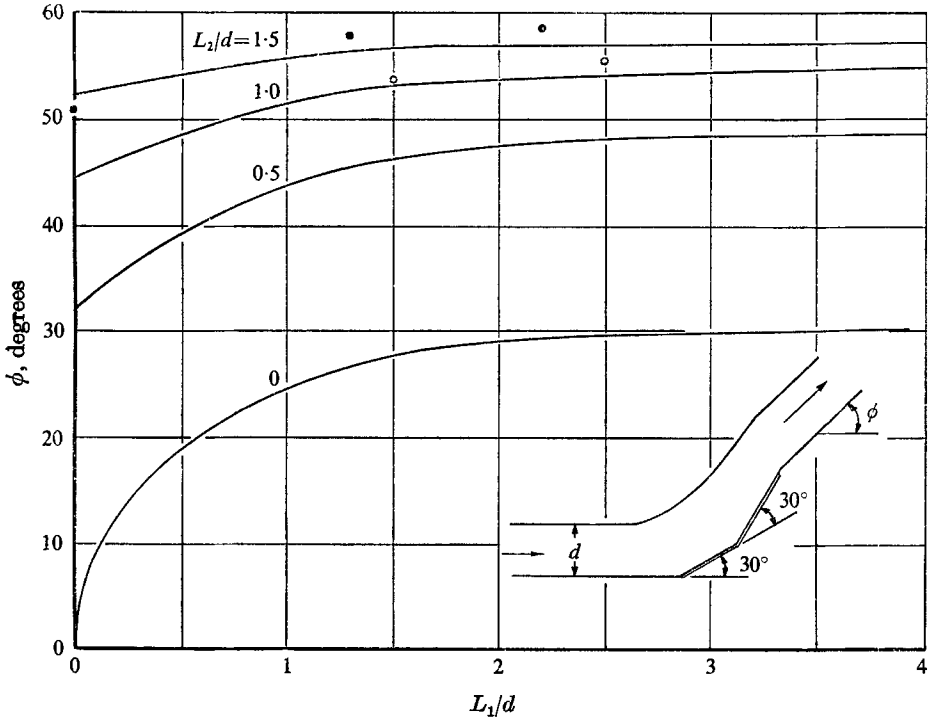

FIGURE 4. Deflexion angle as a function of segmental length for two-segment case with $\alpha_1 = \alpha_2 = 30°$. Experimental points from Copp: ○, $L_2/d = 1{\cdot}0$; ●, $L_2/d = 1{\cdot}5$.

case when $\alpha_1 = \alpha_2 = 90°$; those by Tinney *et al.* are for $\alpha_1 = \alpha_2$. Computer results were produced by the authors for these special cases for comparison. Again, the agreement is extremely good. Experimental data obtained by Siao & Hubbard for the one-segment deflector and those by Copp (1960) for the two-segment deflector are also plotted.

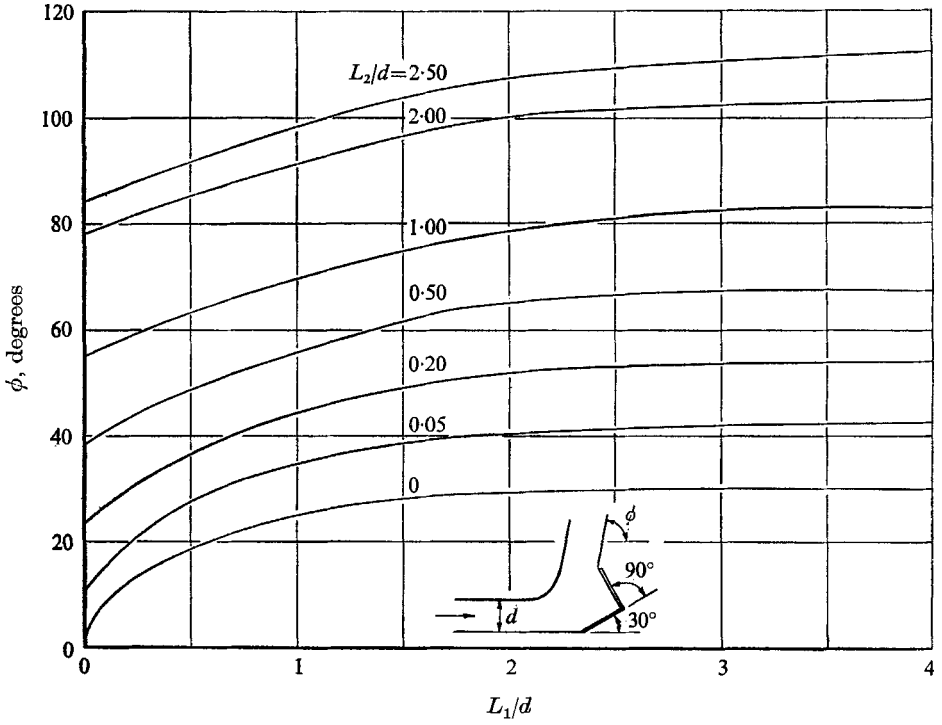

FIGURE 5. Deflexion angle as a function of segmental length for two-segment case with $\alpha_1 = 30°$ and $\alpha_2 = 90°$.

The authors are grateful for the assistance in computer work by Mr Joseph J. Housman and Mr David T. Zemer of San Diego State College.

Appendix. Evaluation of integrals

'Runge–Kutta method' may be used to evaluate the integrals where they are applicable, but it is evident that it fails at the singular point. The following approximate method, which was originally developed by Bryan & Jones (1915) will consequently be used near the singular point. As an example, consider the integral for the two-segment case

$$\int_{A_2}^{\frac{1}{2}\pi} \left[\frac{\sin(U+A_1)}{\sin(U-A_1)}\right]^{\alpha_1/\pi} \left[\frac{\sin(U+A_2)}{\sin(U-A_2)}\right]^{\alpha_2/\pi} \cot U \, dU,$$

where $U = A_2$ is the singular point.

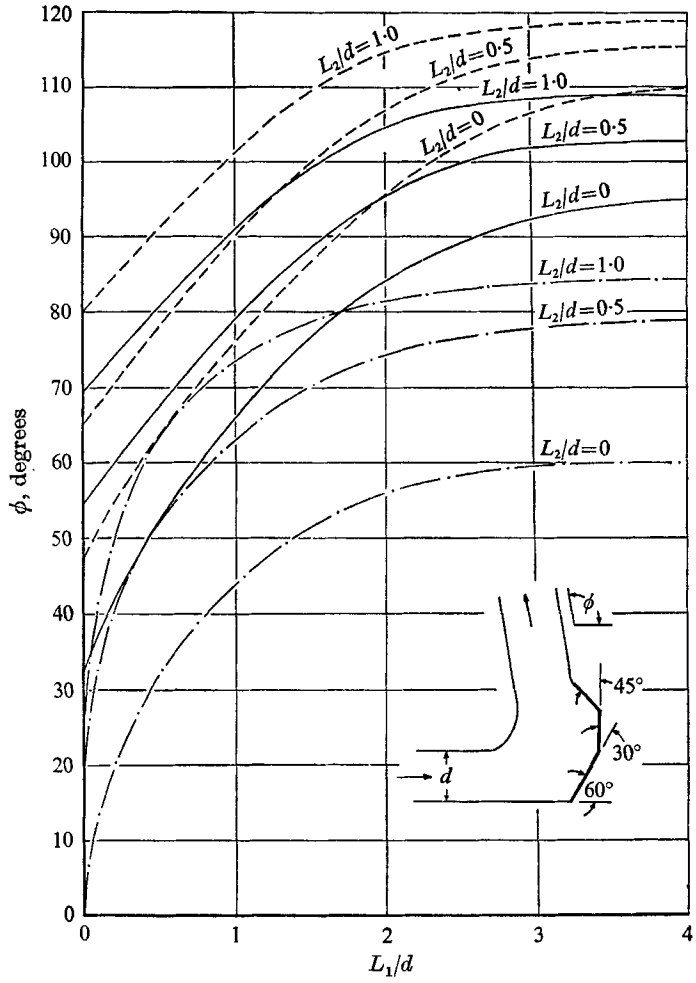

FIGURE 6. Deflexion angle as a function of segmental length for three-segment case with $\alpha_1 = 60°$, $\alpha_2 = 30°$ and $\alpha_3 = 45°$. – – –, $L_3/d = 1{\cdot}0$; —, $L_3/d = 0{\cdot}5$; — · —, $L_3/d = 0$.

Set $U - A_2 = \chi$, $\alpha_1/\pi = \mu$ and $\alpha_2/\pi = \nu$; the integral becomes

$$\frac{1}{\sin^{\nu}\chi}\left[\frac{\sin^{\mu}(A_1+A_2+\chi)\sin^{\nu}(2A_2+\chi)\cot(A_2+\chi)}{\sin^{\mu}(A_2-A_1+\chi)}\right] = F(\chi).$$

When $\chi \to 0$ (i.e. $U \to A_2$), $\sin^{\mu}\chi \to \chi^{\mu}$, and we may write $F(\chi) = \chi^m \phi(\chi)$, where $m = -\mu$. $\phi(\chi)$ is now expended in powers of χ, being finite and continuous within the limits, and

$$F(\chi) = A\chi^m + B\chi^{m+1} + C\chi^{m+2} + \ldots = y. \tag{A1}$$

Let

y_1 be the value of $y[= F(\chi)]$ when $\chi = h$,

y_2 be the value of $y[= F(\chi)]$ when $\chi = 2h$,

$\vdots$

y_r be the value of $y[= F(\chi)]$ when $\chi = rh$.

Suppose

$$\begin{aligned}\int_0^{rh} y\,d\chi \text{ (to be required)} &= (P_1y_1+P_2y_2+\ \dots\ +P_ry_r)h\\ &= P_1(Ah^m+Bh^{m+1}+Ch^{m+2}+\ \dots\ )h\\ &\quad +P_2[A(2h)^m+B(2h)^{m+1}+C(2h)^{m+2}+\ \dots]h+\ \dots\\ &\quad +P_r[A(rh)^m+B(rh)^{m+1}+C(rh)^{m+2}+\ \dots]h\\ &= (P_1+2^mP_2+\ \dots\ +r^mP_r)Ah^{m+1}\\ &\quad +(P_1+2^{m+1}P_2+\ \dots\ +r^{m+1}P_r)Bh^{m+2}\\ &\quad +(P_1+2^{m+2}P_2+\ \dots\ +r^{m+2}P_r)Ch^{m+3}+\ \dots.\end{aligned}$$

But if we integrate (A 1), it becomes

$$\int_0^{rh} y\,d\chi = \frac{A(rh)^{m+1}}{m+1}+\frac{B(rh)^{m+2}}{m+2}+\frac{C(rh)^{m+3}}{m+3}+\ \dots.$$

Therefore

$$P_1+2^mP_2+\ \dots\ +r^mP_r = r^{m+1}/m+1,$$

$$P_1+2^{m+1}P_2+\ \dots\ +r^{m+1}P_r = r^{m+2}/m+2, \text{ and so on,}$$

which, when solved, gives the values of P's.

In our case the lengths have been calculated for different values of μ and ν, and r has been taken to be 2, giving then

$$P_1 = \frac{2^{m+2}}{(m+1)(m+2)} = \frac{2^{2-\nu}}{(1-\nu)(2-\nu)}, \tag{A 2}$$

$$P_2 = \frac{2m}{(m+1)(m+2)} = \frac{-2\nu}{(1-\nu)(2-\nu)}, \tag{A 3}$$

and

$$\int_0^{2h} F(\chi)d\chi = (P_1y_1+P_2y_2)h. \tag{A 4}$$

The formula derived here, then, will be used in the immediate vicinity of A_1 and A_2, from A_1 to A_1' say, along the first segment; $0 < A_1 < A_1'$; from A_2' to A_2 along the first segment; $A_1' < A_2' < A_2$; and from A_2 to A_2'' along the second segment; $A_2 < A_2'' < \frac{1}{2}\pi$. The values of the integrals from A_1' to A_2' and from A_2'' to $\frac{1}{2}\pi$ will be evaluated according to the Runge–Kutta method.

To test the accuracy of this procedure, the integral

$$\int_0^a \frac{d\chi}{(a^2-\chi^2)^{\frac{1}{2}}}$$

has been evaluated and found to be 1·55, as compared with the true value $\frac{1}{2}\pi = 1{\cdot}57$. The error is, therefore, about 1·5 % with these intervals.

REFERENCES

BRYAN, G. H. & JONES, R. 1915 Discontinuous fluid motion past a bent plane, with special reference to aeroplane problems. *Proc. Roy. Soc.* A **91**, 354–70.

CHANG, H. Y. 1968 Flow analysis inside thrust reversers. *Engineering Report* 24–2287, Rohr Corp., Chula Vista, California.

COPP, H. D. 1960 Laboratory investigations on trajectories from segmental flip buckets. M.S. Thesis, Washington State University.

SARPKAYA, T. 1953 Deflexion of jets, II, symmetrically placed U-shaped obstacle. *Studies in Engineering*, 35, State University of Iowa.

SIAO, T. T. & HUBBARD, P. G. 1953 Deflexion of jets, I, symmetrically placed V-shaped obstacle. *Studies in Engineering*, 35, State University of Iowa.

TINNEY, E. R., BARNES, W. E., RECHARD, O. W. & INGRAM, G. R. 1961 Free-streamline theory for segmental jet deflectors. *J. Hydraul. Div. Am. Soc. Civ. Engrs*, HY **5**, 135–145.